Electrochemical Lithiation and Delithiation Properties of Ceria–Coated Silicon Electrodes

Yasuhiro Domi,[a,b] Hiroyuki Usui,[a,b] Hodaka Itoh,[a,b] Hiroki Sakaguchi[a,b,*]

[a] Department of Chemistry and Biotechnology, Graduate School of Engineering, and [b] Center for Research on Green Sustainable Chemistry, Tottori University, Minami 4–101, Koyama–cho, Tottori 680–8552, Japan

* Corresponding Author: Hiroki Sakaguchi

Tel: +81–857–31–5265, fax: +81–857–31–5265

E–mail address: sakaguch@chem.tottori–u.ac.jp

Abstract

The effect of a ceria (CeO_2) coating on the electrochemical performance of a Si negative electrode for use in lithium–ion batteries was investigated. The results of X–ray diffraction analysis, field–emission scanning electron microscopy, and energy–dispersive X–ray spectroscopy showed that CeO_2 uniformly coated the entire surface of Si particles. The CeO_2–coated Si electrode showed better cyclability than a Si electrode, and the cycle performance of CeO_2–coated Si electrode improved with an increase in the coating amount of CeO_2. The CeO_2/Si (15:85 wt.%) electrode maintained a greater discharge capacity at around the 400th cycle, whereas the capacity of the Si electrode began to decay under capacity limitation. While Si–alone and CeO_2–coated electrodes had almost the same surface roughness before cycling, the surface roughness of the Si electrode was about 1.6 times greater than that of the CeO_2/Si (15:85 wt.%) electrode after the 30th cycle; disintegration of the Si–alone electrode was suppressed by CeO_2–coating.

Keywords: lithium–ion battery; silicon; ceria; rare–earth compound; gas deposition.

1. Introduction

Silicon (Si) materials are promising candidates as negative electrodes for lithium–ion batteries (LIBs) due to their high theoretical capacity (3580 mA h g^{-1} for $Li_{15}Si_4$), abundance, and low cost [1,2]. However, Si has several issues such as a significant change in volume during the alloying (charge) and dealloying (discharge) processes with Li, poor electrical conductivity, and a low diffusion coefficient for Li^+ [3,4]; a Si negative electrode shows poor cycle performance. To address these issues, various approaches have been proposed, including the preparation of a nanostructured material of Si to buffer volume expansion [5–8], the application of film–forming additives or ionic liquid electrolytes to form a stable surface film and/or to improve the safety of LIBs [9–13], the coating of Si with a conductive material to reduce the electrical resistivity [14,15], and the doping of Si with impurities, such as boron, phosphorous, or arsenic, to increase the electrical conductivity of Si and/or to change its properties regarding morphology, phase transition, and crystallinity [16–22].

Our previous studies have demonstrated that composite electrodes consisting of elemental Si and a rare–earth metal silicide or a base–metal silicide are effective for addressing the above issues [23–25]. We also reported that a coating of rutile TiO_2 on Si electrodes improves their electrochemical performance [26], which indicates that the

formation of a composite with oxide materials may improve the electrochemical performance of Si. In this study, we focused on the fact that CeO_2 has a higher standard Gibbs energy of formation (–1025 kJ mol^{-1}) than rutile TiO_2 (–890 kJ mol^{-1}) [27]; CeO_2 is more thermodynamically stable than rutile TiO_2 and is therefore less likely to decompose under repeated charge/discharge cycles. The effect of a CeO_2 coating on the electrochemical performance of a Si electrode was investigated.

2. Experimental

CeO_2–coated Si powder was synthesized by a precipitation method. 25 mL of triethylene glycol dimethyl ether (triglyme, $C_8H_{18}O_4$, Kishida Chemical Co. Ltd., 98%) was added to a stirred solution of $Ce(NO_3)_3 \cdot 6H_2O$ (77 mg, 0.18 mmol) in 50 mL of water at 55°C, and the solution was stirred for 1 h. 0.38 or 0.14 g of Si powder (Wako Pure Chemical Industries, Ltd.), which was mechanically milled for 10 min, was added to the solution to form CeO_2/Si (5:95 wt.%) or CeO_2/Si (15:85 wt.%), respectively. 1 mL of NH_4OH (Kishida Chemical Co. Ltd., 28%) was then added and the solution was stirred at 50°C for 1.5 h. CeO_2 is thought to be formed by the reaction of $Ce(OH)_3$ with dissolved oxygen and then deposits on the Si particle surface. The precipitate was filtered off, washed with water, dried in vacuo for 24 h, and heated under vacuum at 400°C for 4 h.

For the synthesis of a CeO_2–alone powder, Si powder was not added to the solution. The ratio of Ce to Si was investigated by Energy–dispersive X–ray Fluorescence (ED–XRF, EDX–720, Shimadzu). X–ray diffraction (XRD, Ultima IV, Rigaku) analysis was performed at a voltage of 40 kV and a current of 40 mA with Cu–Kα (λ = 1.5406 Å) radiation to estimate the crystal structure of the powders. The Inorganic Crystal Structure Database (ICSD) was used to identify the obtained XRD patterns. The morphology of CeO_2–coated Si powder was observed by field–emission scanning electron microscopy (FE–SEM) (JSM–6701F, JEOL Co., Ltd.). The surface of the powder was coated with gold to prevent a buildup of charge. Root–mean–square roughness (Rq) of the electrodes was estimated using confocal laser scanning microscopy (CLSM, VK–9700, Keyence).

Electrochemical measurements were carried out using a laboratory–made beaker–type three–electrode cell. The working electrode was fabricated by a gas deposition (GD) method in a vacuum chamber. The GD procedure was as follows; a Cu current collector with a thickness of 20 μm was set at a distance of 10 mm from a nozzle in the chamber. The nozzle (diameter of 0.8 mm) was connected to the end of a guide tube. An aerosol consisting of He gas with a purity of 99.9999% and active material powder was generated in the guide tube, and sprayed from the nozzle onto the Cu substrate in with a base pressure of several tens of Pa (differential pressure of 7.0×10^5

Pa). Both the counter and reference electrodes consisted of Li metal sheets (Rare Metallic, 99.9%, thickness; 1 mm). The electrolyte solution used was 1 M lithium bis(trifluoromethanesulfonyl)amide (LiTFSA) in propylene carbonate (PC; $C_4H_6O_3$, Kishida Chemical Co., Ltd.). The cell was assembled in an Ar–filled glovebox (Miwa MFG, DBO–2.5LNKP–TS) with a dew point below –100°C and an oxygen content below 1 ppm. A galvanostatic charge–discharge test was performed using an electrochemical measurement system (HJ–1001SD8, Hokuto Denko Co., Ltd. or BS2506, KEISOKUKI) in a potential range between 0.005 and 3.000 V vs. Li^+/Li at 303 K under a constant current rate of 1 *C*. In this study, 1 *C* was defined as 3.6, 3.4, and 3.0 A g^{-1} for the Si–alone, CeO_2/Si (5:95 wt.%), and CeO_2/Si (15:85 wt.%) electrodes, respectively.

3. Results and Discussion

To verify that Si particles were coated with CeO_2, an XRD measurement was performed. Figure 1 shows XRD patterns of CeO_2 and CeO_2/Si (15:85 wt.%) powders. The resulting pattern for CeO_2 was in good agreement with the ICSD pattern (00–034–0394), which indicates that the precipitation method gives a single phase of CeO_2. Peaks assigned to CeO_2 (111), CeO_2 (220), and CeO_2 (311) were shifted toward to a lower angle for CeO_2/Si (15:85 wt.%) powder. Since the ICSD pattern of Si (00–026–1481) is at a

slightly lower angle than that of CeO_2, CeO_2/Si (15:85 wt.%) is considered to consist of a mixture of CeO_2 and Si. Figure 2a shows a FE–SEM image of the CeO_2/Si (15:85 wt.%) powder, and Figures 2b and 2c show the corresponding energy–dispersive X–ray spectroscopy (EDS) mapping of Si and Ce, respectively. The results of FE–SEM and EDS mapping demonstrated that CeO_2 was uniformly deposited over the entire surface of Si particles and the size of the deposited CeO_2 was 49 ± 25 nm.

Figures 3a and 3b show the first charge–discharge (lithiation–delithiation) curve of a CeO_2–alone electrode in 1 M LiTFSA/PC at a constant current density of 0.15 A g^{-1} (1 *C*) and the cycle performance, respectively. FE–SEM observation clarified that the particle size of CeO_2 on the electrode was 55 ± 23 nm, which is almost the same as that of CeO_2 on Si (data not shown); i.e., the addition of Si particles did not affect the particle size of CeO_2. Gradual slopes were observed in the charge and discharge curves below 1.9 V and over 1.0 V vs. Li^+/Li, respectively. Lithiation and delithiation reactions of CeO_2 should occur in these potential ranges [28]. Based on Figure 3b, it is obvious that the CeO_2–alone electrode has a superior long–term cycle stability of 1000 cycles, while the discharge capacity is low (less than 100 mA h g^{-1}).

Figure 4 shows charge–discharge curves of Si and CeO_2/Si (5:95 or 15:85 wt.%) electrodes during the first cycle in 1 M LiTFSA/PC. In every case, potential plateaus were

observed in the charge and discharge curves at around 0.1 and 0.4 V vs. Li^+/Li, respectively. These plateaus are attributed to the alloying and dealloying reactions of Si with Li [29,30]. The charge–discharge reactions of the CeO_2/Si (5:95 or 15:85 wt.%) electrode are considered to occur through the CeO_2 layer on the surface.

Figure 5a shows the cycle performance of the Si–alone and CeO_2/Si (5:95 or 15:85 wt.%) electrodes in 1 M LiTFSA/PC at a constant current rate of 1 *C*. This figure also shows the dependence of the discharge capacity on the cycle number for the Si electrode at a constant charge capacity of 500 mA h g^{-1}. The performance of a TiO_2/Si (43:57 wt.%) electrode at 1.6 *C* is shown for comparison. Figure 5b shows the initial Coulombic efficiency of these electrodes. While the Si–alone electrode exhibited a relatively large discharge capacity of ca. 2000 mA h g^{-1} in the initial cycle, it showed a rapid decay of the capacity up to the 100th cycle; the Si electrode has very poor cycle performance. Si shows a significant change in volume during alloying/dealloying reactions with Li, and the expansion ratio of the specific volume from Si to $Si_{15}Li_4$ reaches approximately 380 % [31]. Therefore, this capacity fading likely arises from the change in volume of Si, which causes disintegration of the electrode and/or the pulverization of Si particles. On the other hand, the cycle performance of the CeO_2–coated Si electrode improved with an increase in the coating amount of CeO_2; the discharge capacities of

CeO_2/Si (5:95 wt.%) and CeO_2/Si (15:85 wt.%) electrodes were 180 and 460 mA h g^{-1} at the 500th cycle, respectively. To clarify whether this improvement is due solely to the prevention of Si from alloying with Li and suppression of the change in volume of Si, the cyclability of a Si electrode in 1 M LiTFSA/PC at a fixed lithiation level of 500 mA h g^{-1} was investigated. At around the 400th cycle, when the discharge capacity of the Si–alone electrode began to decay under capacity limitation, the CeO_2/Si (15:85 wt.%) electrode maintained a greater discharge capacity regardless of the large change in volume of Si in CeO_2/Si (15:85 wt.%). These results indicate that CeO_2 does not prevent Si from alloying with Li, but rather suppresses disintegration of the electrode.

It is well known that a surface film forms through reductive decomposition of the electrolyte solution during the initial cycle, and that formation of this film contributes to the decrease in Coulombic efficiency. The resulting film should be break up with the large change in the volume of Si, and a surface film should form again on the newly exposed Si surface. Consequently, the efficiency of the Si–alone electrode decreases in the initial cycle, as shown in Figure 5b. On the other hand, there was no decrease in the initial efficiency of not only the CeO_2/Si (5:95 or 15:85 wt.%) and TiO_2/Si (43:57 wt.%) electrodes, but also the Si–alone electrode under capacity limitation, which indicates that the volumetric change was suppressed and the surface film was not disrupted.

The cycle performance of the CeO_2–coated Si electrode at 1 *C* is inferior to that of a TiO_2–coated Si electrode even at 1.6 *C*, despite its higher standard Gibbs energy of formation (–1025 kJ mol^{-1}); the discharge capacity of the CeO_2/Si (15:85 wt.%) electrode was 460 mA h g^{-1} at the 500th cycle, whereas that of the TiO_2/Si (43:57 wt.%) electrode was 970 mA h g^{-1}. The diffusion coefficient of Li^+ is ca. 10^{-6} and 10^{-12} cm^2 s^{-1} for TiO_2 and CeO_2, respectively [32,33]. Consequently, the diffusion capability of an oxide coating material is thought to influence the cyclability of a Si negative electrode for use in LIBs in preference to the thermodynamic stability.

Figure 6 shows CLSM images of Si and CeO_2/Si (15:85 wt.%) electrodes after the 30th cycle. Based on Figure 6, the Rq values of the Si and CeO_2/Si (15:85 wt.%) electrodes were estimated to be 4.02 and 2.53 μm, respectively, while those before cycling were almost the same (Si: 0.43 μm, CeO_2/Si (15:85 wt.%): 0.47 μm). Therefore, the disintegration of the Si–alone electrode was considered to be suppressed by CeO_2–coating. For the Si–alone electrode, the lithiation reaction occurs locally in limited areas, as shown in Figure 7A, which leads to severe disintegration of the Si electrode and poor cycle performance [34]. On the other hand, the CeO_2– and TiO_2–coated Si electrodes can modestly avoid the accumulation of stress in localized regions due to the uniform lithiation over the entire electrode surface (Figure 7B), which results from their higher

diffusion coefficients for Li^+. Hence, the severe disintegration of the Si electrode and subsequent rapid capacity fading ought to be suppressed.

4. Conclusion

Electrochemical lithiation and delithiation properties of CeO_2–coated Si negative electrodes for use in LIBs were studied. The results of XRD, FE–SEM, and EDS mapping demonstrated that CeO_2 uniformly coated the entire surface of Si particles. The CeO_2–coated Si electrode showed better cycle performance than the Si–alone electrode, and the cyclability of the coated Si electrode improved with an increase in the coating amount of CeO_2; the discharge capacity of the CeO_2/Si (15:85 wt.%) electrode was 460 mA h g^{-1} at the 500th cycle, whereas that of the CeO_2/Si (5:95 wt.%) electrode was 180 mA h g^{-1}. After the 30th cycle, Rq of the Si electrode was about 1.6 times greater than that of the CeO_2/Si (15:85 wt.%) electrode; i.e., disintegration of the Si–alone electrode was suppressed by CeO_2–coating.

Acknowledgements

This work was partially supported by the Japan Society for the Promotion of Science (JSPS) KAKENHI Grant numbers 24350094, 15K21166 and 16K05954. This work was also supported partially by the Electric Technology Research Foundation of Chugoku.

References

[1] Y. Jin, S. Zhang, B. Zhu, Y. Tan, X. Hu, L. Zong, J. Zhu, Simultaneous purification and perforation of low–grade Si sources for lithium–ion battery anode, Nano Lett. 15 (2015) 7742–7747.

[2] J. Wang, D.–H. Liu, Y.–Y. Wang, B.–H. Hou, J.– P. Zhang, R.–S. Wang, Z.–L. Wu, Dual–carbon enhanced silicon–based composite as superior anode material for lithium ion batteries, J. Power Sources 307 (2016) 738–745.

[3] N. Ding, J. Xu, Y. X. Yao, G. Wegner, X. Fang, C. H. Chen, I. Lieberwirth, Determination of the diffusion coefficient of lithium ions in nano–Si, Solid State Ionics 180 (2009) 222–225.

[4] J. Xie, N. Imanishi, T. Zhang, A. Hirano, Y. Takeda, O. Yamamoto, Li–ion diffusion in amorphous Si films prepared by RF magnetron sputtering: A comparison of using liquid and polymer electrolytes, Mater. Chem. Phys. 120 (2010) 421–425.

[5] C. K. Chan, R. N. Patel, M. J. O'Connell, B. A. Korgel, Y. Cui, Solution–grown silicon nanowires for lithium–ion battery anodes, ACS Nano 4 (2010) 1443–1450.

[6] X. Zhou, L.–J. Wan, Y.–G. Guo, Electrospun silicon nanoparticle/porous carbon hybrid nanofibers for lithium–ion batteries, Small 9 (2013) 2684–2688.

[7] X. Liu, Y. Du, L. Hu, X. Zhou, Y. Li, Z. Dai, J. Bao, Understanding the effect of different polymeric surfactants on enhancing the silicon/reduced graphene oxide anode performance, J. Phys. Chem. C 119 (2015) 5848–5854.

[8] J. Ryu, D. Hong, S. Choi, S. Park, Synthesis of ultrathin Si nanosheets from natural clays for lithium–ion battery anodes, ACS Nano 10 (2016) 2843–2851.

[9] Y. Domi, H. Usui, M. Shimizu, K. Miwa, H. Sakaguchi, Effect of film–forming additive on electrochemical performance of silicon negative–electrode in lithium–ion batteries, Int. J. Electrochem. Sci. 10 (2015) 9678–9686.

[10] C. C. Nguyen, S.–W. Song, Characterization of SEI layer formed on high performance Si–Cu anode in ionic liquid battery electrolyte, Electrochem. Commun. 12 (2010) 1593–1595.

[11] V. Baranchugov, E. Markevich, E. Pollak, G. Salitra, D. Aurbach, Amorphous silicon thin films as a high capacity anodes for Li–ion batteries in ionic liquid electrolytes, Electrochem. Commun. 9 (2007) 796–800.

[12] T. Sugimoto, Y. Atsumi, M. Kono, M. Kikuta, E. Ishiko, M. Yamagata, M. Ishikawa, Application of bis(fluorosulfonyl)imide–based ionic liquid electrolyte to silicon–nickel–carbon composite anode for lithium–ion batteries, J. Power Sources 195 (2010) 6153–6156.

[13] C. C. Nguyen, S.–W. Woo, S.–W. Song, Understanding the interfacial processes at silicon–copper electrodes in ionic liquid battery electrolyte, J. Phys. Chem. C 116 (2012) 14764–14771.

[14] J. W. Kim, J. H. Ryu, K. T. Lee, S. M. Oh, Improvement of silicon powder negative electrodes by copper electroless deposition for lithium secondary batteries, J. Power Sources 147 (2005) 227–233.

[15] X. Zhou, Y.–X. Yin, A.–M. Cao, L.–J. Wan, Y.–G. Guo, Efficient 3D conducting networks built by graphene sheets and carbon nanoparticles for high–performance silicon anode, ACS Appl. Mater. Interfaces 4 (2012) 2824–2828.

[16] Y. Domi, H. Usui, M. Shimizu, Y. Kakimoto, H. Sakaguchi, Effect of phosphorus–doping on electrochemical performance of silicon negative electrode in lithium–ion batteries, ACS Appl. Mater. Interfaces 8 (2016) 7125–7132.

[17] J.–H. Noh, K.–Y. Lee, J.–K. Lee, Electrochemical characteristics of phosphorus doped Si–C composite for anode active material of lithium secondary batteries, Trans. Nonferrous Met. Soc. China 19 (2009) 1018–1022.

[18] B. R. Long, M. K. Y. Chan, J. P. Greeley, A. A. Gewirth, Dopant modulated Li insertion in Si for battery anodes: theory and experiment, J. Phys. Chem. C 115 (2011) 18916–18921.

[19] Z. Yang, D. Wang, F. Li, H. Yue, D. Liu, X. Li, L. Qiao, D. He, Copper nanorods supported phosphorus–doped silicon for lithium storage application, Mater. Lett. 117 (2014) 58–61.

[20] S. Rousselot, M. Gauthier, D. Mazouzi, B. Lestriez, D. Guyomard, L. Roué, Synthesis of boron–doped Si particles by ball milling and application in Li–ion batteries, J. Power Sources 202 (2012) 262–268.

[21] R. Yi, J. Zai, F. Dai, M. L. Gordin, D. Wang, Improved rate capability of Si–C composite anodes by boron doping for lithium–ion batteries, Electrochem. Commun. 36 (2013) 29–32.

[22] W. McSweeney, O. Lotty, C. Glynn, H. Geaney, J. D. Holmes, C. O'Dwyer, The influence of carrier density and doping type on lithium insertion and extraction processes at silicon surfaces, Electrochim. Acta 135 (2014) 356–367.

[23] H. Usui, K. Maebara, K. Nakai, H. Sakaguchi, Anode properties of composite thick–film electrodes consisted of Si and various metal silicides, Int. J. Electrochem. Sci. 6 (2011) 2246–2254.

[24] H. Usui, M. Nomura, H. Nishino, M. Kusatsu, T. Murota, H. Sakaguchi, Gadolinium silicide/silicon composite with excellent high–rate performance as lithium–ion battery anode, Mater. Lett. 130 (2014) 61–64.

[25] Y. Domi, H. Usui, Y. Takemoto, K. Yamaguchi, H. Sakaguchi, Improved electrochemical performance of lanthanum silicide/silicon composite electrode with nickel substitution for lithium–ion batteries, J. Phys. Chem. C 120 (2016) 16333–16339.

[26] H. Usui, K. Wasada, M. Shimizu, H. Sakaguchi, TiO_2/Si composites synthesized by sol–gel method and their improved electrode performance as Li–ion battery anodes, Electrochim. Acta 111 (2013) 575–580.

[27] James G. Speight, Lange's Handbook of Chemistry, 17th ed., Laramie, Wyoming, 2016.

[28] C. Hua, X. Fang, Z. Yang, Y. Gao, Z. Wang, L. Chen, Lithium storage mechanism and catalytic behavior of CeO_2, Electrochem. Commun. 25 (2012) 66–69.

[29] Y.–M. Kang, S.–M. Lee, S.–J. Kim, G.–J. Jeong, M.–S. Sung, W.–U. Choi, S.–S. Kim, Phase transitions explanatory of the electrochemical degradation mechanism of Si based materials, Electrochem. Commun. 9 (2007) 959–964.

[30] V. L. Chevrier, J. W. Zwanziger, J. R. Dahn, First principles study of Li–Si crystalline phases: charge transfer, electronic structure, and lattice vibrations, J. Alloy Compd. 496 (2010) 25–36.

[31] M. N. Obrovac, L. J. Krause, Reversible cycling of crystalline silicon powder, J. Electrochem. Soc. 154 (2007) A103–A108.

[32] Y.–S. Hu, L. Kienle, Y.–G. Guo, J. Maier, High lithium electroactivity of nanometer–sized rutile TiO_2, Adv. Mater. 18 (2006) 1421–1426.

[33] A Siokou, S. Ntais, V. Dracopoulos, S. Papaefthimiou, G. Leftheriotis, P. Yianoulis, Substrate related structural, electronic and electrochemical properties of evaporated CeO_x ion storage layers, Thin Solid Films 514 (2006) 87–96.

[34] M. Shimizu, H. Usui, T. Suzumura, H. Sakaguchi, Analysis of the deterioration mechanism of Si electrode as a Li-ion battery anode using Raman microscopy, J. Phys. Chem. C 119 (2015) 2975–2982.

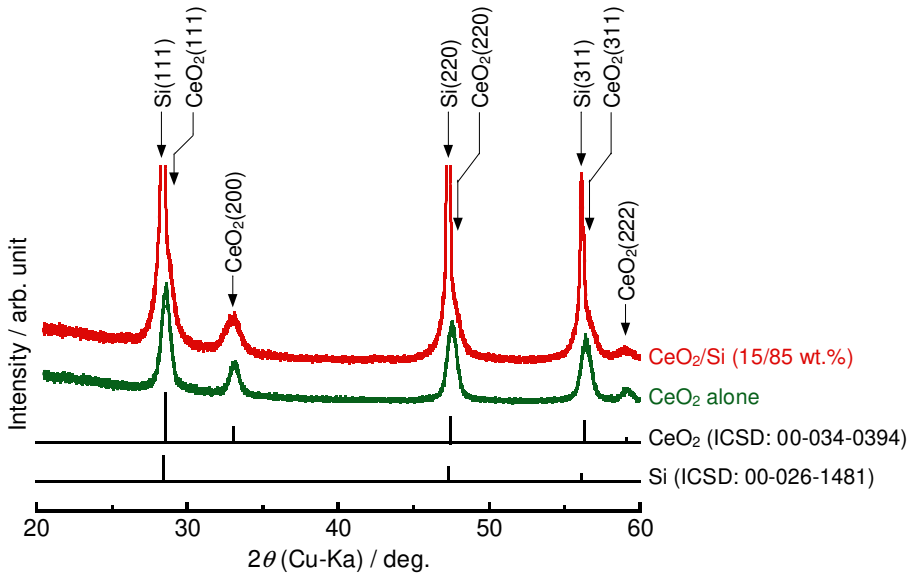

Fig. 1. XRD patterns of CeO_2 and CeO_2/Si (15:85, wt.%) powders synthesized by the precipitation method.

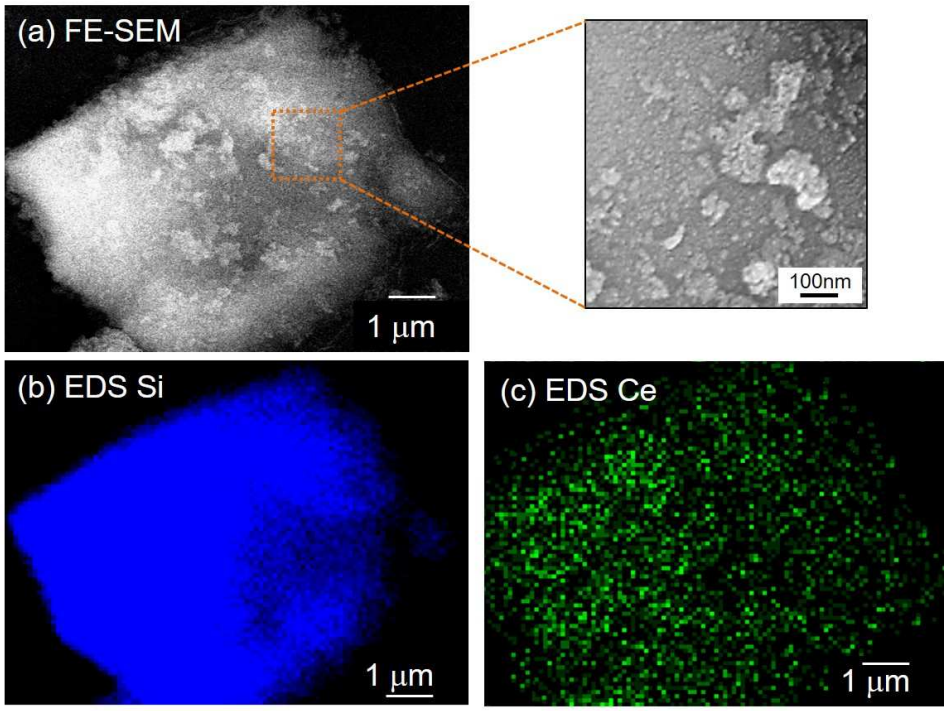

Fig. 2. (a) FE–SEM image, and (b) Si and (c) Ce EDS elemental mappings of CeO_2/Si (15:85 wt.%) powder.

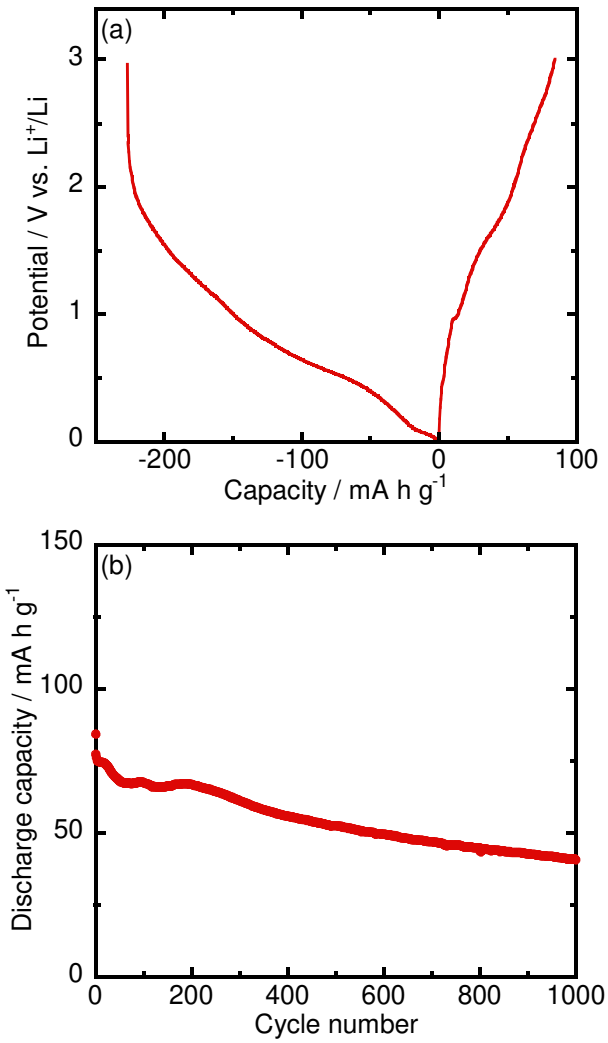

Fig. 3. (a) First charge–discharge curve and (b) cycle performance of CeO_2–alone electrode in 1 M LiTFSA/PC at a constant current density of 0.15 A g^{-1} (1 *C*).

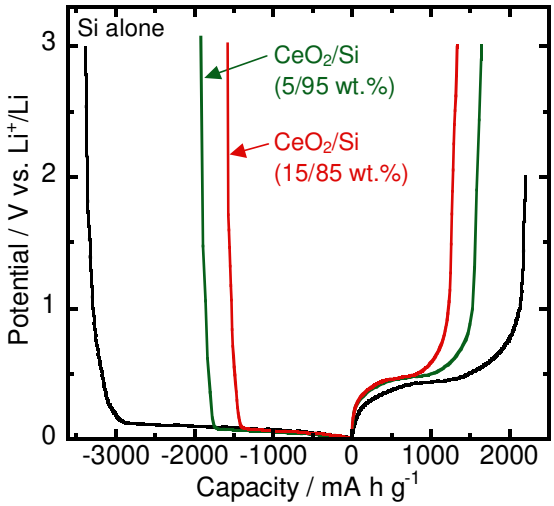

Fig. 4. First charge–discharge curves of Si and CeO_2/Si (5:95 or 15:85 wt.%) electrodes in 1 M LiTFSA/PC at a constant current rate of 1 *C* (current density: 3.6, 3.4, and 3.0 A g^{-1} for Si–alone, CeO_2/Si (5:95 wt.%), and CeO_2/Si (15:85 wt.%) electrodes, respectively).

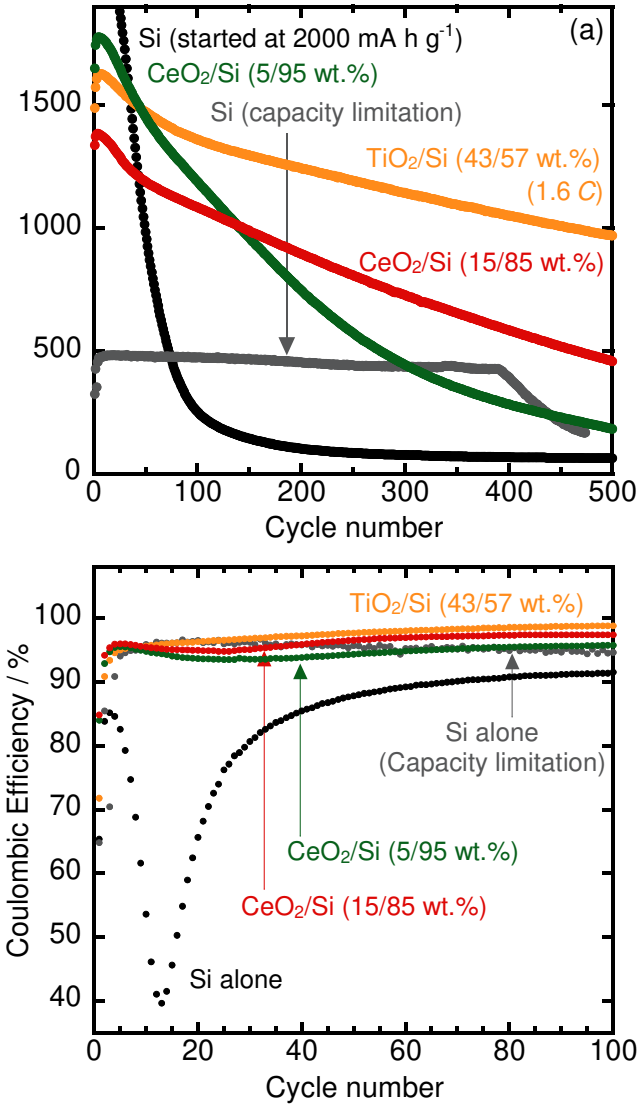

Fig. 5. (a) Cycle performance of Si, CeO_2/Si (5:95 or 15:85 wt.%), and TiO_2/Si (43:57 wt.%) electrodes in 1 M LiTFSA/PC and (b) the initial Coulombic efficiency at a constant current rate of 1 *C*, except for the TiO_2/Si (43:57 wt.%) electrode.

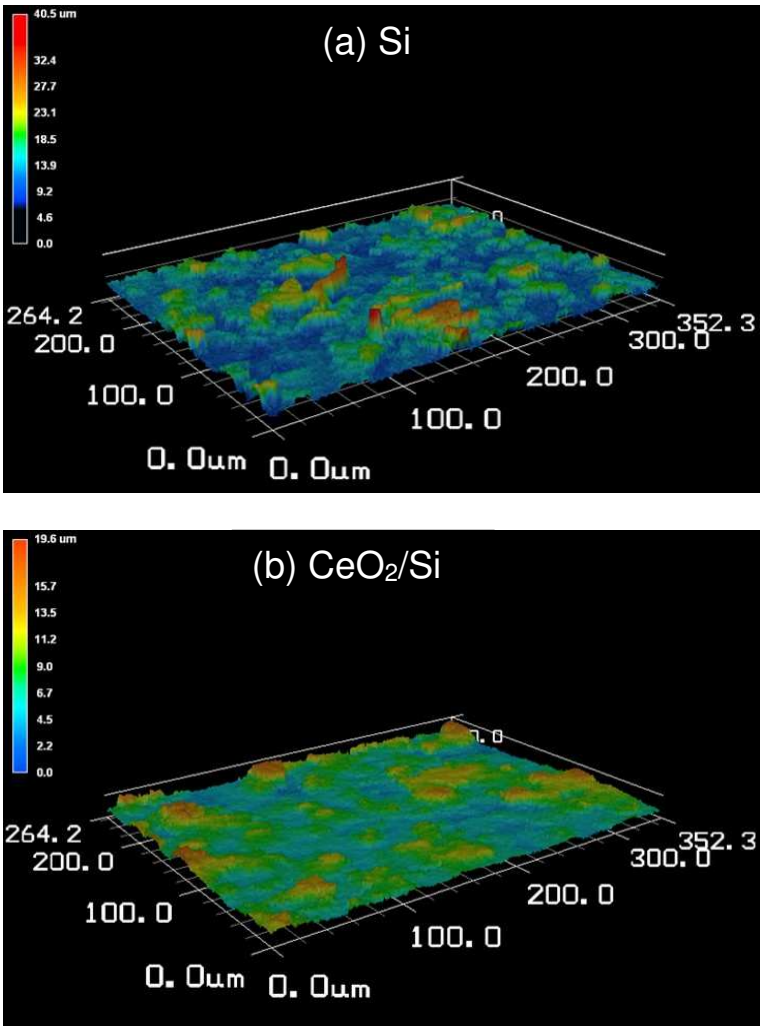

Fig. 6. CLSM images of (a) Si and (b) CeO_2/Si (15:85 wt.%) electrodes after the 30th cycle in 1 M LiTFSA/PC.

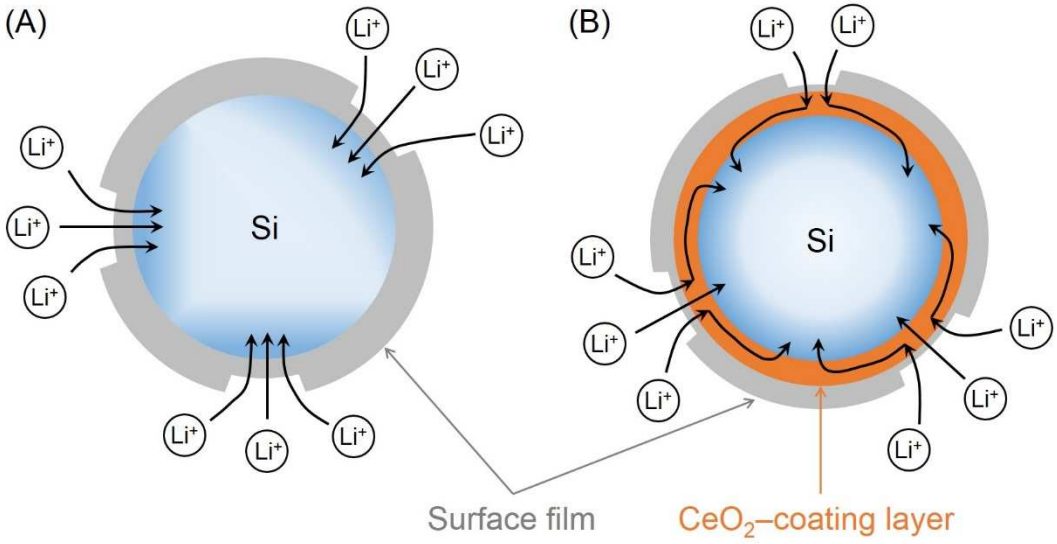

Fig. 7. Schematic illustration of the mechanism of lithiation for (A) Si-alone and (B) CeO_2–coated Si particles.